J. Phys. A: Math. Gen. **32** (1999) 6727–6739. Printed in the UK PII: S0305-4470(99)05029-5

# Nonlinear dynamics of a damped magnetic oscillator

Sang-Yoon Kim
Department of Physics, Kangwon National University, Chunchon, Kangwon-Do 200-701, Korea
E-mail: sykim@cc.kangwon.ac.kr

Received 9 June 1999, in final form 23 July 1999

**Abstract.** We consider a damped magnetic oscillator (MO), consisting of a permanent magnet in a periodically oscillating magnetic field. A detailed investigation of the dynamics of this dissipative magnetic system is made by varying the field amplitude $A$. As $A$ is increased, the damped MO, albeit simple looking, exhibits rich dynamical behaviours such as symmetry-breaking pitchfork bifurcations, period-doubling transitions to chaos, symmetry-restoring attractor-merging crises, and saddle-node bifurcations giving rise to new periodic attractors. Besides these familiar behaviours, a cascade of 'resurrections' (i.e., an infinite sequence of alternating restabilizations and destabilizations) of the stationary points also occurs. It is found that the stationary points restabilize (destabilize) through alternating subcritical (supercritical) period-doubling and pitchfork bifurcations. We also discuss the critical behaviours in the period-doubling cascades.

## 1. Introduction

We consider a permanent magnet of dipole moment $m$ placed in a periodically oscillating magnetic field. This magnetic oscillator (MO) can be described by a second-order non-autonomous ordinary differential equation [1–3],

$$I\ddot{\theta} + b\dot{\theta} + mB\cos\omega t\sin\theta = 0 \tag{1}$$

where the overdots denote the differentiation with respect to time, $\theta$ is the angle between the permanent magnet and the magnetic field, $I$ is the moment of inertia about a rotation axis, $b$ is the damping parameter, and $B$ and $\omega$ are the amplitude and frequency of the periodically oscillating magnetic field, respectively.

Making the normalization $\omega t \rightarrow 2\pi(t + \frac{1}{2})$ and $\theta \rightarrow 2\pi x$, we obtain a dimensionless form of equation (1),

$$\ddot{x} + \Gamma\dot{x} - A\cos 2\pi t\sin 2\pi x = 0 \tag{2}$$

where $x$ is a normalized angle with mod 1, $\Gamma = 2\pi b/I\omega$ and $A = 2\pi mB/I\omega^2$. Note also, that equation (2) describes the motion of a particle in a standing wave field [4–6]. For the conservative case of $\Gamma = 0$, the Hamiltonian system exhibits period-doubling bifurcations and large-scale stochasticity as the normalized field amplitude $A$ is increased, which have been found both experimentally [1–3] and theoretically [4–6]. Here we are interested in the damped case of $\Gamma \neq 0$ and make a detailed investigation of the dynamical behaviours of the damped MO by varying the normalized amplitude $A$.

This paper is organized as follows. We first discuss bifurcations associated with stability of periodic orbits and Lyapunov exponents in the damped MO in section 2. With increasing $A$ up to sufficently large values, dynamical behaviours of the damped MO are then investigated in section 3. This very simple-looking damped MO shows a richness in its dynamical behaviours. As $A$ is increased, breakdown of symmetries via pitchfork bifurcations [7], period-doubling transitions to chaos [8], restoration of symmetries via attractor-merging crises [9], the birth of new periodic attractors through saddle-node bifurcations [7], and so on are numerically found. In addition to these familiar behaviours, the stationary points exhibit a cascade of 'resurrections' [10] (i.e., they restabilize after their instability, destabilize again, and so forth, *ad infinitum*). It is found that the restabilizations (destabilizations) occur via alternating subcritical (supercritical) period-doubling and pitchfork bifurcations. An infinite sequence of period-doubling bifurcations, leading to chaos, also follows each destabilization of the stationary points. In section 4, we also study the critical scaling behaviours in the period-doubling cascades. It is found that the critical behaviours are the same as those for the one-dimensional (1D) maps [8]. Finally, a summary is given in section 5.

## 2. Stability, bifurcations and Lyapunov exponents

In this section we first discuss the stability of periodic orbits in the damped MO, using the Floquet theory [11]. Bifurcations associated with the stability and Lyapunov exponents are then discussed.

The second-order ordinary differential equation (2) is reduced to two first-order ordinary differential equations:

$$\dot{x} = y \tag{3a}$$

$$\dot{y} = -\Gamma y + A\cos 2\pi t \sin 2\pi x. \tag{3b}$$

These equations have two symmetries $S_1$ and $S_2$, because the transformations

$$S_1 : x \to x \pm \tfrac{1}{2} \qquad y \to y \qquad t \to t \pm \tfrac{1}{2} \tag{4}$$

$$S_2 : x \to -x \qquad y \to -y \qquad t \to t \tag{5}$$

leave equation (3) invariant. The transformations in equations (4) and (5) are just the shift in both $x$ and $t$ and the (space) inversion, respectively. Hereafter, we will call $S_1$ and $S_2$ the shift and inversion symmetries, respectively. If an orbit $z(t)$ $(\equiv (x(y), y(t)))$ is invariant under $S_i$ $(i = 1, 2)$, it is called an $S_i$-symmetric orbit. Otherwise, it is called an $S_i$-asymmetric orbit and has its 'conjugate' orbit $S_i z(t)$.

The phase space of the damped MO is three-dimensional with the coordinates $x$, $y$, and $t$. Since the damped MO is periodic in $t$, it is convenient to regard time as a circular coordinate (with mod 1) in the phase space. We then consider the surface of section, the $x$–$y$ plane at integer times (i.e., $t = m$, $m$: integer). The phase-space trajectiory intersects this plane in a sequence of points. This sequence of points corresponds to a mapping on the plane. This map plot of an initial point $z_0$ $(= (x_0, y_0))$ can be conveniently generated by sampling the orbit points $z_m$ at the discrete time $t = m$. We call the transformation $z_m \to z_{m+1}$ the Poincaré map and write $z_{m+1} = P(z_m)$.

The linear stability of a $q$-periodic orbit of $P$, such that $P^q(z_0) = z_0$, is determined from the linearized-map matrix $DP^q(z_0)$ of $P^q$ at an orbit point $z_0$. Here $P^q$ means the $q$-times iterated map. Using the Floquet theory, the matrix $M$ $(\equiv DP^q)$ can be obtained by integrating the linearized equations for small displacements,

$$\delta\dot{x} = \delta y \tag{6a}$$

$$\delta\dot{y} = -\Gamma\delta y + 2\pi A\cos 2\pi t \cos 2\pi x \delta x \tag{6b}$$

with two initial displacements $(\delta x, \delta y) = (1, 0)$ and $(0, 1)$ over the period $q$. The eigenvalues, $\lambda_1$ and $\lambda_2$, of $M$ are called the Floquet (stability) multipliers, characterizing the orbit stability.

By using the Liouville formula [12], we obtain the determinant of $M$ (det $M$),

$$\det M = e^{-\Gamma q}. \tag{7}$$

Hence, the pair of Floquet multipliers of a periodic orbit lies either on the circle of radius $e^{-\Gamma q/2}$ or on the real axis in the complex plane. The periodic orbit is stable when both multipliers lie inside the unit circle. We first note that they never cross the unit circle, except at the real axis and hence Hopf bifurcations do not occur. Consequently, it can lose its stability only when a Floquet multiplier decreases (increases) through $-1$ (1) on the real axis. When a Floquet multiplier $\lambda$ decreases through $-1$, the periodic orbit loses its stability via period-doubling bifurcation. On the other hand, when a Floquet multiplier $\lambda$ increases through 1, it becomes unstable via pitchfork or saddle-node bifurcation. For each case of the period-doubling and pitchfork bifurcations, two types of supercritical and subcritical bifurcations occur. For more details on bifurcations, we refer the reader to [7].

Lyapunov exponents of an orbit $\{z_m\}$ in the Poincaré map $P$, characterize the mean exponential rate of divergence of nearby orbits [13]. There exist two Lyapunov exponents $\sigma_1$ and $\sigma_2$ ($\sigma_1 \geqslant \sigma_2$) such that $\sigma_1 + \sigma_2 = -\Gamma$, because the linearized Poincaré map $DP$ has a constant Jacobian determinant, $\det DP = e^{-\Gamma}$. We choose an initial perturbation $\delta z_0$ to the initial orbit point $z_0$ and iterate the linearized map $DP$ for $\delta z$ along the orbit to obtain the magnitude $d_m$ ($\equiv |\delta z_m|$) of $\delta z_m$. Then, for almost all infinitesimally small initial perturbations, we have the largest Lyapunov exponent $\sigma_1$ given by

$$\sigma_1 = \lim_{m\to\infty} \frac{1}{m} \ln \frac{d_m}{d_0}. \tag{8}$$

If $\sigma_1$ is positive, then the orbit is called a chaotic orbit; otherwise, it is called a regular orbit.

## 3. Rich dynamical behaviours of the damped MO

In this section, by varying the normalized amplitude $A$, we investigate the evolutions of both the stationary points and the rotational orbits of period 1 in the damped MO for a moderately damped case of $\Gamma = 1.38$. As $A$ is increased, the damped MO, albeit simple looking, exhibits rich dynamical behaviours, such as symmetry-breaking pitchfork bifurcations, period-doubling transitions to chaos, symmetry-restoring attractor-merging crises, and saddle-node bifurcations giving rise to new periodic attractors. In addition to these familiar behaviours, the stationary points also undergo a cascade of resurrections (i.e. an infinite sequence of alternating restabilizations and destabilizations). It is found that the restabilizations (destabilizations) occur via alternating subcritical (supercritical) period-doubling and pitchfork bifurcations. An infinite sequence of period-doubling bifurcations, leading to chaos, also follows each destabilization of the stationary points.

### *3.1. Evolution of the stationary points*

We first consider the case of the stationary points. The damped MO has two stationary $\hat{z}$ points. One is $\hat{z}_I = (0, 0)$, and the other one is $\hat{z}_{II} = (\frac{1}{2}, 0)$. These stationary points are symmetric ones with respect to the inversion symmetry $S_2$, while they are asymmetric and conjugate ones with respect to the shift symmetry $S_1$. Hence they are partially symmetric orbits with only the inversion symmetry $S_2$. We also note that the two stationary points are the fixed points of the Poincaré map $P$ (i.e. $P(\hat{z}) = \hat{z}$ ($\hat{z} = \hat{z}_I, \hat{z}_{II}$)).

With increasing $A$ we investigate the evolution of the two fixed points $\hat{z}_I$ and $\hat{z}_{II}$. Two bifurcation diagrams starting from $\hat{z}_I$ and $\hat{z}_{II}$ are given in figures 1(*a*) and (*b*), respectively. Each fixed point loses its stability via symmetry-conserving period-doubling bifurcation,

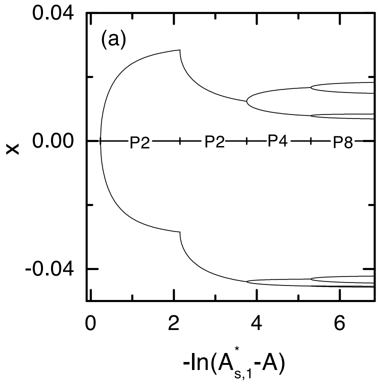


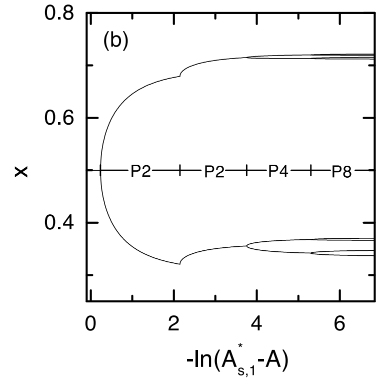


**Figure 1.** Bifurcation diagrams starting from (*a*) the $S_2$-symmetric, but $S_1$-asymmetric, stationary point $\hat{z}_I$ and (*b*) its $S_1$-conjugate stationary point $\hat{z}_{II}$. The first and second P2s denote the stable $A$-ranges of the $S_2$-symmetric and $S_2$-asymmetric orbits of period 2, respectively. The other P$N$ ($N = 4, 8$) also designates the stable $A$-range of the $S_2$-asymmetric periodic orbit with period $N$.

giving rise to a stable $S_2$-symmetric orbit with period 2. However, as $A$ is further increased each $S_2$-symmetric orbit of period 2 becomes unstable by a symmetry-breaking pitchfork bifurcation, leading to the birth of a conjugate pair of $S_2$-asymmetric orbits of period 2. (For the sake of convenience, only one $S_2$-asymmetric orbit of period 2 is shown.) After breakdown of the $S_2$ symmetry, each 2-periodic orbit with completely broken symmetries exhibits an infinite sequence of period-doubling bifurcations, ending at a finite critical point $A^*_{s,1}$ ($= 3.934\,787\ldots$). The critical scaling behaviours near the critical point $A^*_{s,1}$ are the same as those for the 1D maps [8], as we see in section 4.

After the period-doubling transition to chaos, four small chaotic attractors with completely broken symmetries appear; they are related with respect to the two symmetries $S_1$ and $S_2$. As $A$ is increased the different parts of each chaotic attractor coalease and form larger pieces. For example, two chaotic attractors with $\sigma_1$ (largest Lyapunov exponent) $\simeq 0.11$, denoted by $c_1$ and $c_2$, near the unstable stationary point $\hat{z}_I$ are shown in figure 2(*a*) for $A = 3.937$; their conjugate chaotic attractors with respect to the $S_1$ symmetry near the unstable stationary point $\hat{z}_{II}$ are not shown. Each one is composed of four distinct pieces. However, as $A$ is further increased these pieces also merge into two larger pieces. An example with $\sigma_1 \simeq 0.18$ is shown in figure 2(*b*) for $A = 3.94$.

As $A$ exceeds a critical value ($\simeq$3.9484), the two chaotic attractors $c_1$ and $c_2$ in figure 2(*b*) merge into a larger one, $c$, through an $S_2$-symmetry-restoring attractor-merging crisis. For example, a chaotic attractor $c$ with $\sigma_1 \simeq 0.37$ and its conjugate one, denoted by $s$, with respect to the $S_1$ symmetry are shown in figure 3(*a*) for $A = 3.96$. These two chaotic attractors $c$ and $s$ are $S_2$-symmetric ones, although they are still $S_1$-asymmetric and conjugate ones. Thus

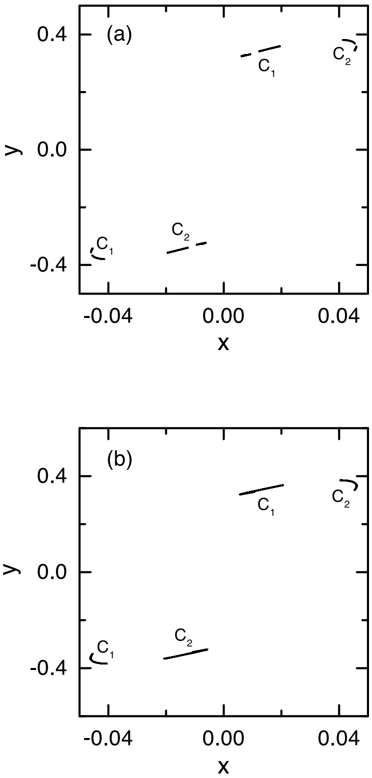


**Figure 2.** Band-merging of chaotic attractors. (*a*) For $A = 3.937$, each of the chaotic attractors $c_1$ and $c_2$ is composed of four pieces. However, as $A$ is increased these pieces also merge to form two larger pieces. An example for $A = 3.94$ is shown in (*b*).

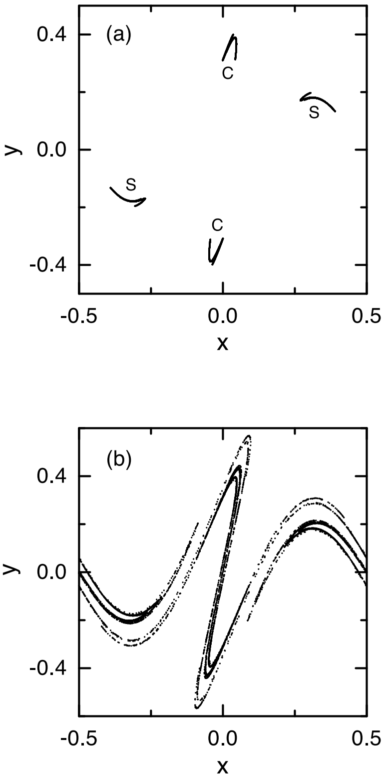


**Figure 3.** Attractor-merging crises. The two chaotic attractors $c_1$ and $c_2$ in figure 2(*b*) merge into a larger one $c$ via $S_2$-symmetry-restoring crisis. For $A = 3.96$ the chaotic attractor $c$ with the inversion symmetry $S_2$ and its conjugate one $s$ with respect to the $S_1$ symmetry are shown in (*a*). These two $S_1$-asymmetric small chaotic attractors $c$ and $s$ also merge to form a larger one via $S_1$-symmetry-restoring crisis. A single large chaotic attractor with completely restored $S_1$ and $S_2$ symmetries is shown in (*b*) for $A = 3.98$.

the inversion symmetry $S_2$ is first restored. However, as $A$ increases through a second critical value ($\simeq$3.9672), the two small chaotic attractors $c$ and $s$ also merge into a larger one via $S_1$-symmetry-restoring attractor-merging crisis, as shown in figure 3(*b*) for $A = 3.98$. Note that the single large chaotic attractor with $\sigma \simeq 0.64$ is both the $S_1$- and $S_2$-symmetric one. Consequently, the two symmetries $S_1$ and $S_2$ are completely restored, one by one through two successive symmetry-restoring attractor-merging crises. However, this large chaotic attractor disappears for $A \simeq 4.513$, and then the system is asymptotically attracted to a stable rotational orbit of period 1 born through a saddle-node bifurcation, as shown in figure 4.

### *3.2. Evolution of the rotational orbits*

We now investigate the evolution of the rotational orbits of period 1. A pair of stable and unstable rotational orbits with period 1 is born for $A \simeq 2.771$ via saddle-node bifurcation. In contrast to the stationary points, these rotational orbits are $S_1$-symmetric, but $S_2$-asymmetric

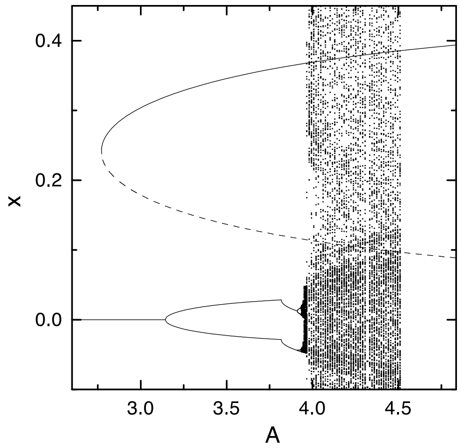


**Figure 4.** Jump to a rotational orbit. The large symmetric chaotic attractor in figure 3(*b*) disappears for $A \simeq 4.513$, and then the asymptotic state of the damped MO becomes a stable rotational orbit with period 1 born via saddle-node bifurcation. Such a saddle-node bifurcation, giving rise to a pair of stable and unstable orbits of period 1, occurs for $A \simeq 2.771$ (a stable orbit is denoted by a solid curve, while an unstable one is represented by a dashed curve). A bifurcation diagram starting from $\hat{z}_I$ is also shown.

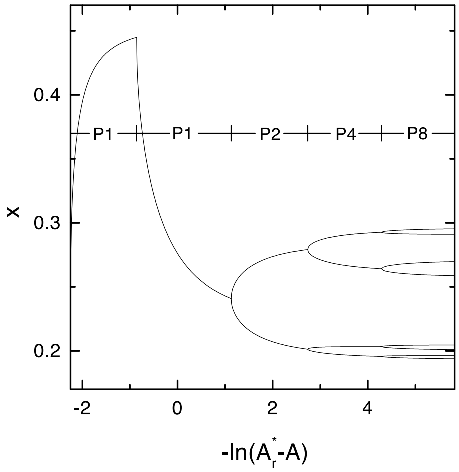


**Figure 5.** Bifurcation diagram starting from the $S_1$-symmetric, but $S_2$-asymmetric, rotational orbit with period 1. The first and second P1s denote the stable $A$-ranges of the $S_1$-symmetric and $S_1$-asymmetric orbits of period 1, respectively. The other P$N$ ($N = 2, 4, 8$) also designates the stable $A$-range of the $S_1$-asymmetric periodic orbit with period $N$.

and conjugate, ones. The bifurcation diagram starting from a stable rotational orbit with positive angular velocity is shown in figure 5. (For convenience, the bifurcation diagram starting from its $S_2$-conjugate rotational orbit with negative angular velocity is omitted.) The $S_1$-symmetric rotational orbit of period 1 becomes unstable by a symmetry-breaking pitchfork bifurcation, which results in the birth of a pair of $S_1$-asymmetric rotational orbits with period 1. (For the sake of convenience, only one $S_1$-asymmetric orbit of period 1 is shown.) Then each rotational orbit with completely broken symmetries undergoes an infinite sequence of period-doubling bifurcations, accumulating at a finite critical point $A_r^*$ ($= 12.252\,903\ldots$). The critical behaviours near the accumulation point $A_r^*$ are also the same as those for the 1D maps, as in the case of the stationary points.

For $A > A_r^*$, four chaotic attractors with completely broken symmetries appear; they are related with respect to the two symmetries $S_1$ and $S_2$. Through a band-merging process, each chaotic attractor eventually becomes composed of a single piece, as shown in figure 6(*a*) for $A = 12.32$. Four chaotic attractors with $\sigma_1 \simeq 0.36$ are denoted by $c_1$, $c_2$, $s_1$, and $s_2$, respectively. However, as $A$ passes through a critical value ($\simeq$12.3424) the four small chaotic attractors merge into a larger one via symmetry-restoring attractor-merging crisis. An example for $A = 12.38$ is given in figure 6(*b*). Note that the single large chaotic attractor with $\sigma_1 \simeq 0.64$ has both the $S_1$ and $S_2$ symmetries. Thus the two symmetries are completely restored through one symmetry-restoring attractor-merging crisis, which is in contrast to the case of the stationary points.

However, as shown in figure 7, the large symmetric chaotic attractor in figure 6(*b*) also disappears for $A \simeq 13.723$, at which saddle-node bifurcations occur. After disappearence of this large chaotic attractor, the system is asymptotically attracted to a stable $S_2$-symmetric, but $S_1$-asymmetric, orbit of period 2 born via saddle-node bifurcation. This stable $S_2$-symmetric

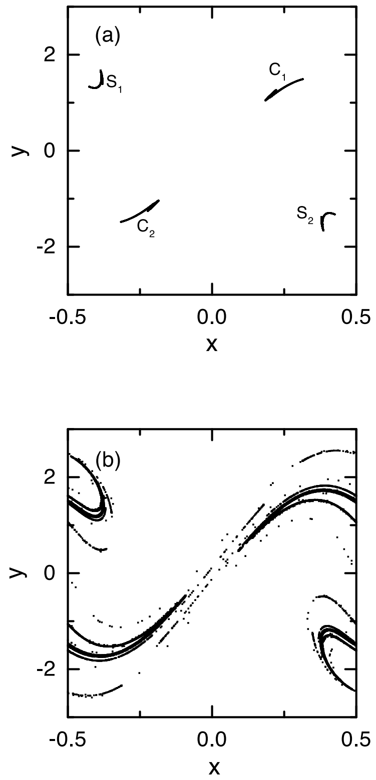


**Figure 6.** Attractor-merging crisis for the rotational case. Through a band-merging process, each of the four chaotic attractors $c_1$, $c_2$, $s_1$, and $s_2$ with completely broken symmetries eventually becomes composed of a single piece, as shown in (*a*) for $A = 12.32$. The four small asymmetric chaotic attractors merge into a larger one via symmetry-restoring crisis. A single large chaotic attractor with simultaneously restored $S_1$ and $S_2$ symmetries is shown in (*b*) for $A = 12.38$.

orbit with period 2 also exhibits rich dynamical behaviours similar to those of the stationary points. That is, as $A$ is increased, a symmetry-breaking pitchfork bifurcation, period-doubling transition to chaos, merging of small asymmetric chaotic attractors into a large symmetric one via symmetry-restoring attractor-merging crisis, and so on are found. However, unlike the cases of the stationary points and the rotational orbits, the large symmetric chaotic attractor disappears for $A = 23.751\,799\ldots$, at which the two unstable stationary points $\hat{z}_I$ and $\hat{z}_{II}$ become restabilized through subcritical period-doubling bifurcations. These 'resurrections' of the stationary points will be described below in some details.

### 3.3. *Resurrections of the stationary points*

The linear stability of the two stationary points $\hat{z}_I$ and $\hat{z}_{II}$ is determined by their linearized equations,

$$\delta\ddot{x} + \Gamma\delta\dot{x} \mp 2\pi A \cos 2\pi t \delta x = 0 \tag{9}$$

where the $-$ (+) sign of the third term corresponds to the case of $\hat{z}_I$ ($\hat{z}_{II}$). (The linearized equation of $\hat{z}_{II}$ can also be transformed into that of $\hat{z}_I$ by just making a shift in time, $t \to t + \frac{1}{2}$.) Note that equation (9) is just a simple form of the more general damped Mathieu equation [14]. It is well known that the Mathieu equation has an infinity of alternating stable and unstable $A$ ranges. Hence, as $A$ is increased, the stationary points undergoes a cascade of 'resurrections,' i.e., they will restabilize after they lose their stability, destabilize again, and so forth, *ad infinitum*.

It is found that their restabilizations (destabilizations) occur through alternating subcritical (supercritical) period-doubling and pitchfork bifurcations. As examples, we consider the

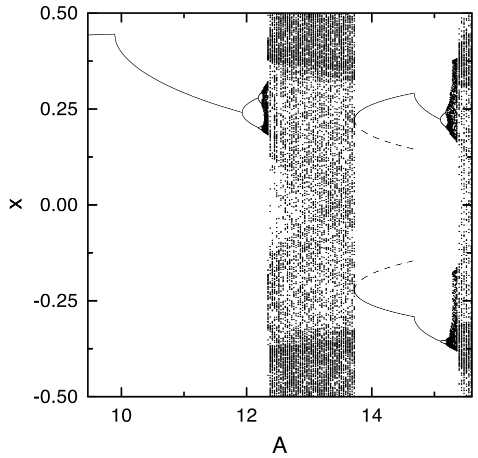


**Figure 7.** Jump to an orbit with period 2. The large symmetric chaotic attractor in figure 6(*b*) disappears for $A \simeq 13.723$, at which a saddle-node bifurcation, giving rise to a pair of stable and unstable orbits with period 2, occurs. (A stable orbit is denoted by a solid curve, while an unstable one is represented by a dashed curve.) Then the damped MO is asymptotically attracted to the stable $S_2$-symmetric, but $S_1$-asymmetric, orbit with period 2. This stable $S_2$-symmetric orbit also exhibits rich dynamical behaviours similar to those of the stationary points. In the left part, a bifurcation diagram starting from a rotational orbit with period 1 is also given.

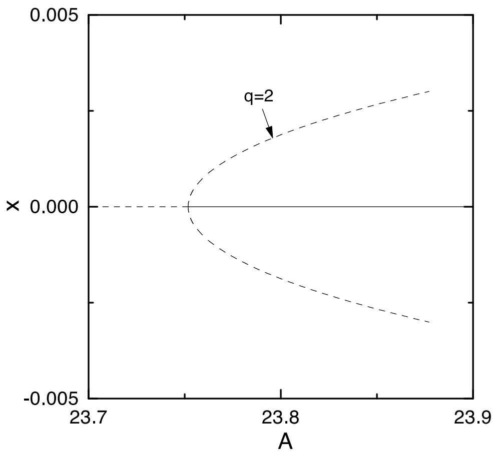


**Figure 8.** First resurrection of the stationary point $\hat{z}_I$. When $A$ passes through the first restabilization value ($\simeq$23.752), the unstable stationary point $\hat{z}_I$ restabilizes through a subcritical period-doubling bifurcation, giving rise to an unstable orbit with period $q = 2$. The solid line and dashed curves also denote stable and unstable orbits, respectively.

first and second resurrections of the stationary points. The first resurrection of $\hat{z}_I$ is shown in figure 8. When $A$ passes through the first restabilization value ($= 23.751\,799\ldots$), the rightmost large symmetric chaotic attractor in figure 7 disappears and the unstable stationary point $\hat{z}_I$ restabilizes via subcritical period-doubling bifurcation, giving rise to an unstable orbit of period 2. Two bifurcation diagrams starting from the restabilized $\hat{z}_I$ and $\hat{z}_{II}$ are given in figures 9(*a*) and (*b*), respectively. Each stationary point loses its stability via symmetry-breaking pitchfork bifurcation, giving rise to a pair of $S_2$-asymmetric orbits with period 1; only one asymmetric 1-periodic orbit is shown. This is in contrast to the case given in section 3.1 (cf figures 1 and 9), where the stationary points become unstable via symmetry-conserving period-doubling bifurcations. After breakdown of the $S_2$ symmetry, an infinite sequence of period-doubling bifurcations follows and ends at its accumulation point $A^*_{s,2}$ ($= 24.148\,001\ldots$). When $A$ exceeds $A^*_{s,2}$, a second period-doubling transition to chaos occurs. The critical scaling behaviours of period doublings near the second critical point $A = A^*_{s,2}$ are also the same as those near the first critical point $A^*_{s,1}$.

Dynamical behaviours of the damped MO after the second period-doubling transition to chaos are shown in figure 10(*a*). As $A$ passes through a critical value ($\simeq$24.1549), small chaotic attractors with completely broken symmetries merge into a large symmetric chaotic attractor via symmetry-restoring attractor-merging crisis. However, the large chaotic attractor also disappears for $A \simeq 29.342$, at which saddle-node bifurcations occur. After disappearence of the large chaotic attractor, the damped MO is asymptotically attracted to a stable $S_1$-symmetric, but $S_2$-asymmetric, orbit of period 1 born via saddle-node bifrucation. The subsequent evolution of the stable 1-periodic orbit is shown in figure 10(*b*). Note that it is similar to that of the rotational orbit described in section 3.2 (cf figures 10(*b*) and 7).

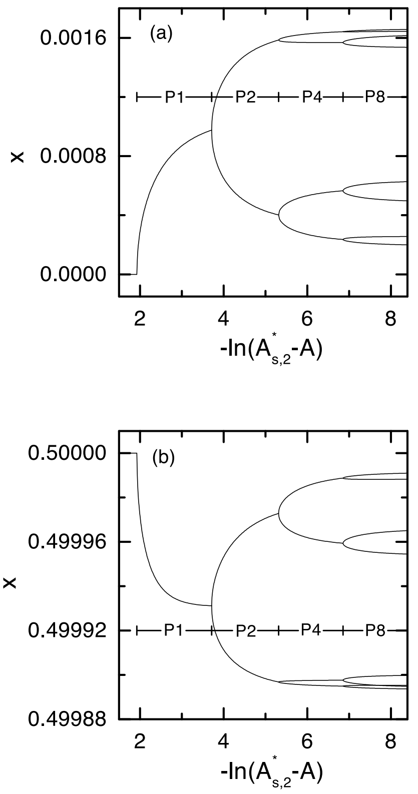


**Figure 9.** Second bifurcation diagrams starting from: (*a*) the restabilized stationary point $\hat{z}_I$ and (*b*) its $S_1$-conjugate stationary point $\hat{z}_{II}$. Here the P$N$ designates the stable $A$-range of the $S_2$-asymmetric periodic orbit with period $N$ ($N = 1, 2, 4, 8$).

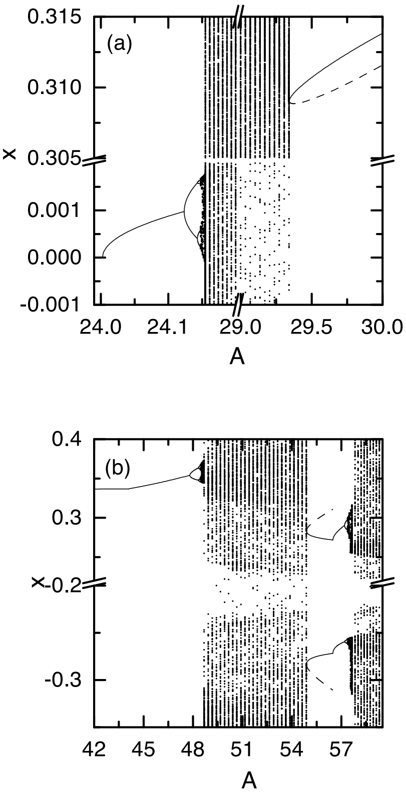


**Figure 10.** Dynamical behaviours after the second period-doubling transition to chaos is shown in (*a*). For $A \simeq 24.1549$ small chaotic attractors with completely broken symmetries merge into a large symmetric chaotic attractor via symmetry-restoring crisis. However, this large symmetric chaotic attractor disappears for $A \simeq 29.342$, and then the damped MO is asymptotically attracted to a stable orbit of period 1 born via saddle-node bifurcation. As shown in (*b*), subsequent evolution of the stable $S_1$-symmetric, but $S_2$-asymmetric, 1-periodic orbit is similar to that of the rotational orbit shown in figure 7. Here the solid and dashed curves also denote stable and unstable orbits, respectively. For other details see text.

The rightmost large symmetric chaotic attractor in figure 10(*b*) appears via symmetry-restoring attractor-merging crisis for $A = 57.67$. However, it also disappears for $A = 67.076\,913\ldots$, at which each stationary point restabilizes again. Unlike the case of the first resurrection (see figure 8), this second resurrection of each stationary point occurs via subcritical pitchfork bifurcation, giving rise to a pair of unstable 1-periodic orbits with broken symmetries. The second resurrections of the two stationary points $\hat{z}_I$ and $\hat{z}_{II}$ and their subsequent bifurcation diagrams are shown in figures 11(*a*) and (*b*), respectively. Note that these third bifurcation diagrams are similar to those in figure 1. The critical scaling behaviours near the third period-doubling transition point $A^*_{s,3}$ ($= 67.104\,872\ldots$) are also the same as those near the first period-doubling transition point $A = A^*_{s,1}$.

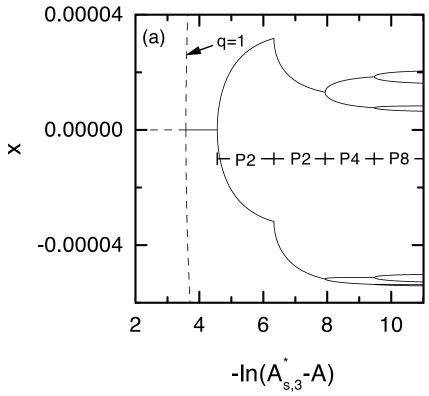


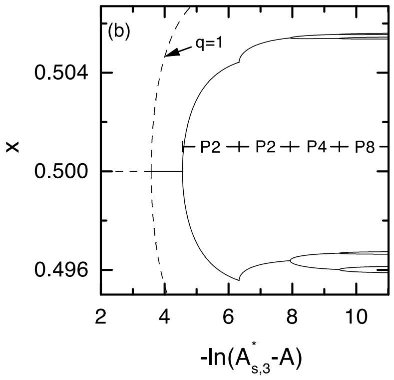


**Figure 11.** Second resurrections of the stationary points and third bifurcation diagrams starting from: (*a*) the restabilized stationary point $\hat{z}_I$ and (*b*) its $S_1$-conjugate stationary point $\hat{z}_{II}$. When $A$ passes through the second restabiliztion value ($\simeq$67.08), each unstable stationary point becomes restabilized via subcritical pitchfork bifurcation, giving rise to a pair of unstable orbits with period $q = 1$. The solid and dashed lines represent stable and unstable orbits, respectively. The third bifurcation diagrams are similar to those in figure 1; the symbols are also the same as those of figure 1.

## 4. Critical scaling behaviours in the period-doubling cascades

In this section, we study the critical scaling behaviours in the period-doubling cascades. The orbital scaling behaviour and the power spectra of the periodic orbits born via period-doubling bifurcations as well as the parameter scaling behaviour are particularly investigated.

The critical scaling behaviours for all cases studied are found to be the same as those for the 1D maps. As an example, we consider the first period-doubling transition to chaos for the case of the stationary points. As explained in section 3.1, each stationary point becomes unstable through symmetry-conserving period-doubling bifurcation, giving rise to a stable $S_2$-symmetric orbit of period 2. However, each $S_2$-symmetric orbit of period 2 also becomes unstable via symmetry-breaking pitchfork bifurcation, which results in the birth of a conjugate pair of $S_2$-asymmetric orbits with period 2. Then, each 2-periodic orbit with completely broken symmetries undergoes an infinite sequence of period-doubling bifurcations, ending at its accumulation point $A^*_{s,1}$. Table 1 gives the $A$ values at which the period-doubling bifurcations occur; at $A_k$, a Floquet multiplier of an asymmetric orbit with period $2^k$ becomes $-1$. The sequence of $A_k$ converges geometrically to its limit value $A^*_{s,1}$ with an asymptotic ratio $\delta$:

$$\delta_k = \frac{A_k - A_{k-1}}{A_{k+1} - A_k} \rightarrow \delta. \tag{10}$$

The sequence of $\delta_k$ is also listed in table 1. Note that its limit value $\delta$ ($\simeq$4.67) agrees well with that ($= 4.669\ldots$) for the 1D maps [8]. We also obtain the value of $A^*_{s,1}$ ($= 3.934\,787\,024$) by superconverging the sequence of $\{A_k\}$ [15].

**Table 1.** Asymptotically geometric convergence of the parameter sequence $\{A_k\}$.

| $k$ | $A_k$ | $\delta_k$ |
|---|---|---|
| 1 | 3.911 404 100 371 | |
| 2 | 3.929 795 227 873 | 4.690 |
| 3 | 3.933 716 964 019 | 4.664 |
| 4 | 3.934 557 747 089 | 4.667 |
| 5 | 3.934 737 918 915 | 4.669 |
| 6 | 3.934 776 506 700 | 4.668 |
| 7 | 3.934 784 773 689 | 4.673 |
| 8 | 3.934 786 542 923 | |

**Table 2.** Asymptotically geometric convergence of the orbital sequences $\{x^{(k)}\}$ and $\{y^{(k)}\}$.

| $k$ | $x^{(k)}$ | $\alpha_{x,k}$ | $y^{(k)}$ | $\alpha_{y,k}$ |
|---|---|---|---|---|
| 1 | 0.012 394 993 | | 0.337 125 704 | |
| 2 | 0.016 703 927 | −2.354 | 0.350 786 135 | −3.410 |
| 3 | 0.014 873 276 | −2.607 | 0.346 780 101 | −2.133 |
| 4 | 0.015 575 414 | −2.451 | 0.348 658 607 | −2.714 |
| 5 | 0.015 288 893 | −2.532 | 0.347 966 417 | −2.395 |
| 6 | 0.015 402 057 | −2.487 | 0.348 255 392 | −2.561 |
| 7 | 0.015 356 562 | −2.511 | 0.348 142 575 | −2.472 |
| 8 | 0.015 374 678 | | 0.348 188 212 | |

We note that the normalized amplitude $A$, exhibiting a scaling, is proportional to the magnetic field amplitude $B$ and the inverse square of its frequency $\omega$ (i.e. $A \sim B/\omega^2$, see equation (2)). For the case of a fixed $\omega$, the stationary points undergo period-doubling cascades as $B$ is increased. Irrespective of the fixed value of $\omega$, the sequence of $B_k$ (the values at which the period-doubling bifurcations occur) converges geometrically to its limit value $B^*$ with the same convergence ratio $\delta$, although the value of the accumulation point $B^*$ increases in propotion to the square of the frequency $\omega$.

As in the 1D maps, we are also interested in the orbital scaling behaviour near the most rarified region. Hence, we first locate the most rarified region by choosing an orbit point $z^{(k)}$ $(= (x^{(k)}, y^{(k)}))$ which has the largest distance from its nearest orbit point $P^{2^{k-1}}(z^{(k)})$ for $A = A_k$. The two sequences $\{x^{(k)}\}$ and $\{y^{(k)}\}$, listed in table 2, converge geometrically to their limit values $x^*$ and $y^*$ with the 1D asymptotic ratio $\alpha$ $(= -2.502\ldots)$, respectively:

$$\alpha_{x,k} = \frac{x^{(k)} - x^{(k-1)}}{x^{(k+1)} - x^{(k)}} \to \alpha \qquad \alpha_{y,k} = \frac{y^{(k)} - y^{(k-1)}}{y^{(k+1)} - y^{(k)}} \to \alpha. \tag{11}$$

The values of $x^*$ $(= 0.015\,369)$ and $y^*$ $(= 0.348\,175)$ are also obtained by superconverging the sequences of $x^{(k)}$ and $y^{(k)}$, respectively.

We also study the power spectra of the $2^k$-periodic orbits at the period-doubling bifurcation points $A_k$. Consider the orbit of level $k$ whose period is $q = 2^k$, $\{z_m^{(k)} = (x_m^{(k)}, y_m^{(k)}), m = 0, 1, \ldots, q-1\}$. Then its Fourier component of this $2^k$-periodic orbit is given by

$$z^{(k)}(\omega_j) = \frac{1}{q}\sum_{m=0}^{q-1} z_m^{(k)} \mathrm{e}^{-\mathrm{i}\omega_j m} \tag{12}$$

where $\omega_j = 2\pi j/q$, and $j = 0, 1, \ldots, q-1$. The power spectrum $P^{(k)}(\omega_j)$ of level $k$ defined by

$$P^{(k)}(\omega_j) = |z^{(k)}(\omega_j)|^2 \tag{13}$$

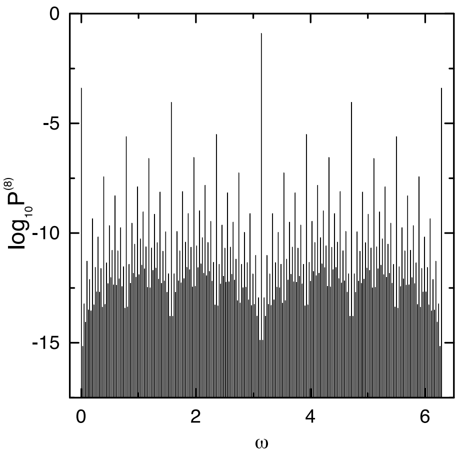


**Figure 12.** Power spectrum $P^{(8)}(\omega)$ of level 8 for $A = A_8$ (= 3.934 786 542 923).

**Table 3.** Sequence $2\beta^{(k)}(l)$ ($\equiv \phi^{(k)}(l)/\phi^{(k)}(l+1)$) of the ratios of the successive average heights of the peaks in the power spectra.

| | $l$ | | | | |
|---|---|---|---|---|---|
| $k$ | 3 | 4 | 5 | 6 | 7 |
| 6 | 18.2 | 22.5 | 21.0 | | |
| 7 | 18.1 | 22.1 | 21.1 | 21.5 | |
| 8 | 18.1 | 22.0 | 20.7 | 21.6 | 21.4 |

has discrete peaks at $\omega = \omega_j$. In the power spectrum of the next $(k+1)$ level, new peaks of the $(k+1)$th generation appear at odd harmonics of the fundamental frequency, $\omega_j = 2\pi(2j+1)/2^{(k+1)}$ ($j = 0, \ldots, 2^k - 1$). To classify the contributions of successive period-doubling bifurcations in the power spectrum of level $k$, we write

$$P^{(k)} = P_{00}\delta(\omega) + \sum_{l=1}^{k} \sum_{j=0}^{2^{(l-1)}-1} P_{lj}^{(k)} \delta(\omega - \omega_{lj}) \tag{14}$$

where $P_{lj}^{(k)}$ is the height of the $j$th peak of the $l$th generation appearing at $\omega = \omega_{lj}$ ($\equiv 2\pi(2j+1)/2^l$). As an example, we consider the power spectrum $P^{(8)}(\omega)$ of level 8 shown in figure 12. The average height of the peaks of the $l$th generation is given by

$$\phi^{(k)}(l) = \frac{1}{2^{(l-1)}} \sum_{j=0}^{2^{l-1}-1} P_{lj}^{(k)}. \tag{15}$$

It is of interest whether or not the sequence of the ratios of the successive average heights

$$2\beta^{(k)}(l) = \phi^{(k)}(l)/\phi^{(k)}(l+1) \tag{16}$$

converges. The ratios are listed in table 3. They seem to approach a limit value, $2\beta \simeq 21$, which also agrees well with that (= 20.96 . . .) for the 1D maps [16].

## 5. Summary

Dynamical behaviours of the moderately-damped MO with $\Gamma = 1.38$ are investigated in detail by varying the normalized amplitude $A$. It is thus found that the damped MO, despite its apparent simplicity, exhibits very rich dynamical behaviours such as diverse bifurcations, chaos, crises and so on. Hence, this MO may serve as a standard example for demonstrative purposes to illustrate the basic ideas of the nonlinear dynamics and chaos. Furthermore, note also that its experimental apparatus, suitable for student laboratory use, can be easily constructed [1–3]. Thus we believe that our work may provide very useful information for such basic experimentation.

Finally, we briefly mention the damping effect. For comparison with the case of moderate damping, we also studied critical scaling behaviour in the period-doubling cascades for two other high and low damping cases of $\Gamma = 10$ and 0.05, respectively. It is thus found that the critical behaviours for both cases of high and low damping becomes eventually the same as those for the moderately damped case, although the weakly damped (nearly Hamiltonian) system with $\Gamma = 0.05$ exhibits a Hamiltonian-like behaviour in a transient way (i.e., a crossover from the Hamilotonian (parameter scaling factor $\delta = 8.721\ldots$ [17]) to dissipative ($\delta = 4.669\ldots$) cases occurs). Hence we believe that our results for the case of moderate damping also becomes valid for the asymptotic dynamics of both the strongly and weakly damped MO.

## Acknowledgments

The author would like to thank K Lee for his assitance in the numerical computations. This work was supported by the Biomedlab Incorporated and by the Korea Research Foundation under Project No 1998-015-D00065.

## References

[1] Croquette V and Poitou C 1981 *J. Physique Lett.* **42** 537
[2] Meissner H and Schmidt G 1986 *Am. J. Phys.* **54** 800
[3] Briggs K 1987 *Am. J. Phys.* **55** 1083
[4] Bialek J, Schmidt G and Wang B H 1985 *Physica* D **14** 265
[5] Schmidt G 1982 *Comment. Plasma Phys. Control. Fusion* **7** 87
[6] Escande D F and Doveil F 1981 *Phys. Lett.* A **83** 307
Escande D F and Doveil F 1981 *J. Stat. Phys.* **26** 257
[7] Guckenheimer J and Holmes P 1983 *Nonlinear Oscillations, Dynamical Systems, and Bifurcations of Vector Fields* (New York: Springer) section 3.5
[8] Feigenbaum M J 1978 *J. Stat. Phys.* **19** 25
Feigenbaum M J 1979 *J. Stat. Phys.* **21** 669
[9] Grebogi C, Ott E, Romeiras F and Yorke J A 1987 *Phys. Rev.* A **36** 5365
[10] Kim S-Y and Lee K 1996 *Phys. Rev.* E **53** 1579
[11] Guckenheimer J and Holmes P 1983 *Nonlinear Oscillations, Dynamical Systems, and Bifurcations of Vector Fields* (New York: Springer) p 24
[12] Arnold V I 1973 *Ordinary Differential Equations* (Cambridge, MA: MIT) p 114
[13] Lichtenberg A J and Lieberman M A 1983 *Regular and Chaotic Dynamics* (New York: Springer) p 262
[14] Morse P M and Feshbach H 1953 *Methods of Theoretical Physics* (New York: McGraw-Hill) section 5.2
Mathews J and Walker R L 1965 *Mathematical Methods of Physics* (New York: Benjamin) section 7.5
[15] MacKay R S 1982 *PhD Thesis* Princeton University (see equations 3.1.2.12 and 3.1.2.13)
[16] Nauenberg M and Rudnick J 1981 *Phys. Rev.* B **24** 493
[17] Greene J M, MacKay R S, Vivaldi F and Feigenbaum M J 1981 *Physica* D **3** 468